Research Article GU J Sci 36(4): 1658-1673 (2023) DOI: 10.35378/gujs.904961

Gazi University

Journal of Science

http://dergipark.gov.tr/gujs

An Adaptive Time Filtered Backward Euler Method for Reduced-Order Models of Incompressible Flows

Fatma G. EROGLU*

Department of Mathematics, Faculty of Science, Bartın University, Bartın 74110, Turkey

Highlights

- This paper focuses on the VMS-POD model of the Navier-Stokes equations
- A filter-based method is introduced that improves the accuracy of the VMS-POD scheme.
- It is presented that the proposed method conserve energy better.

Article Info

Received: 9 Apr 2021
Accepted: 16 Sep 2022

Keywords

Proper orthogonal decomposition, Time filter, Reduced-order models, Projection-based variational multiscale

Abstract

This paper studies a reduced-order model based on proper orthogonal decomposition (POD) for the incompressible Navier-Stokes equations. The difficulties resulting from nonlinearity are eliminated using the variational multiscale (VMS) method. The time filter is added as a separate post-processing step to the standard VMS-POD approximation. This increases the accuracy and presents a better energy preserving scheme without adding additional computational complexity. The stability and error analyses of the method are provided, and results of the several numerical tests are presented to verify the efficiency of the method in this setting.

1. INTRODUCTION

This paper considers the incompressible Navier-Stokes equations (NSE) in the dimensionless form:

$$\begin{aligned} \boldsymbol{u}_t - \nu \Delta \boldsymbol{u} + (\boldsymbol{u} \cdot \nabla)\boldsymbol{u} + \nabla p &= \boldsymbol{f} \quad in \ (0,\tau] \times \Omega, \\ \nabla \cdot \boldsymbol{u} &= 0 \quad in \ (0,\tau] \times \Omega, \\ \boldsymbol{u} &= 0 \quad in \ (0,\tau] \times \Omega, \\ \boldsymbol{u}(0,\boldsymbol{x}) &= \boldsymbol{u}_0 \quad in \ \Omega \end{aligned} \tag{1}$$

where $\boldsymbol{u}(t,\boldsymbol{x})$ and $p(t,\boldsymbol{x})$ are the fluid velocity and the pressure fields, respectively. Let $\Omega \subset \mathbb{R}^d, d \in \{2,3\}$ be a polyhedral domain with a boundary $\partial\Omega$. The parameters in (1) are the initial velocity field $\boldsymbol{u}_0$, prescribed body forces $\boldsymbol{f}(x,t)$ and kinematic viscosity $\nu > 0$, inversely proportional to the Reynolds number, Re.

It is known that the use of direct numerical simulation (DNS) to find a numerical solution of (1) results in large degrees of freedom. This causes high computational cost and complexity. Utilizing Galerkin based reduced-order modelling with proper orthogonal decomposition (POD) is an efficient method for lowering the computational complexity in such settings, [1-3]. POD uses only the most energetic modes from an ensemble of data obtained using the standard Galerkin finite element procedure. Therefore, the application of POD ensures that the complexity, computational cost, and degrees of freedom in the system are

*e-mail: fguler@bartin.edu.tr

significantly reduced. The performance of the approach is improved by the variational multiscale (VMS) method of [4-8], which is based on adding an artificial viscosity term. As VMS affects only resolved small scales, significant reductions appear in the oscillations of the small scales. Since the POD basis functions are given in descending order, the small-resolved scales required for the implementation of the VMS method can be easily decomposed.

Recent studies show that, adding a time filter improves the accuracy of the backward-Euler scheme from first order to second order, and eliminates its over-damping behavior without increasing the complexity of the system, as shown in [9-13] and the references therein. In addition, as discussed in [12], the time filtered backward Euler method gives better energy balance in comparison with the conventional backward Euler method. Hence, in the present work the time filtered backward Euler temporal discretization is utilized and the novel ideas of [11,12] are expanded to the VMS-POD setting for NSE. As the filter is included as a separate post-processing step, the method can be easily incorporated into the existing backward Euler codes.

This paper is organized as follows. In section 2, the notations and preliminaries which will be used for the analysis are given. Section 3 presents the energy conservation, stability, and error analyses. Section 4 includes numerical experiments for validating the presented method. Finally, the paper ends with the conclusions in Section 5.

2. NOTATION AND PRELIMINARIES

The standard Sobolev spaces and their norms are used throughout this paper. The notations $(\cdot,\cdot)$, $||\cdot||$, $||\cdot||_{L^p}$ show the inner product, norm in the $L^2(\Omega)$ space, and norm in the Lebesgue spaces $\left(\left(L^p(\Omega)\right)^d,\ 1 \le p < \infty, p \neq 2\right)$, respectively, [14]. The norm in $\left(H^k(\Omega)\right)^d$ and dual space H^{-1} of $H_0^1(\Omega)$ are given by $||\cdot||_k$ and $||\cdot||_{-1}$, respectively. The continuous velocity, pressure spaces and divergence free space of velocity are given as

$$\boldsymbol{X} := \left(H_0^1(\Omega)\right)^d,\ Q := L_0^2(\Omega),$$

$$\boldsymbol{V} := \{\, \boldsymbol{v} \in \boldsymbol{X} :\ (\nabla \cdot \boldsymbol{v}, q) = 0, \qquad \forall\, q \in Q \,\}.$$

The continuous variational formulation of (1) reads as: Find $\boldsymbol{u} : (0,\tau] \to \boldsymbol{X},\ p : (0,\tau] \to Q$ satisfying

$$(\boldsymbol{u}_t, \boldsymbol{v}) + \nu(\nabla \boldsymbol{u}, \nabla \boldsymbol{v}) + b(\boldsymbol{u}, \boldsymbol{u}, \boldsymbol{v}) - (p, \nabla \cdot \boldsymbol{v}) = (\boldsymbol{f}, \boldsymbol{v}),$$

$$(q, \nabla \cdot \boldsymbol{u}) = 0, \tag{2}$$

for all $(\boldsymbol{v}, q) \in (X, Q)$, where

$$b(\boldsymbol{u}, \boldsymbol{v}, \boldsymbol{w}) := \frac{1}{2}\Big(\big((\boldsymbol{u}\cdot\nabla)\boldsymbol{v}, \boldsymbol{w}\big) - \big((\boldsymbol{u}\cdot\nabla)\boldsymbol{w}, \boldsymbol{v}\big)\Big),$$

represent the skew-symmetric form of the convective term.

Lemma 2.1. The following bounds are provided by the trilinear skew-symmetric form $b(\boldsymbol{u}, \boldsymbol{v}, \boldsymbol{w})$.

$$b(\boldsymbol{u}, \boldsymbol{v}, \boldsymbol{w}) \le M(\Omega)\sqrt{||\boldsymbol{v}||\,||\nabla \boldsymbol{v}||}\ ||\nabla \boldsymbol{v}||\,||\nabla \boldsymbol{w}||,$$

$$b(\boldsymbol{u}, \boldsymbol{v}, \boldsymbol{w}) \le M(\Omega)||\nabla \boldsymbol{u}||\,||\nabla \boldsymbol{v}||\,||\nabla \boldsymbol{w}||,$$

for all $\boldsymbol{u}, \boldsymbol{v}, \boldsymbol{w} \in \boldsymbol{X}$.

Proof. Please see [15] for the proof.

The following notations are used for the discrete norms

$$\left|\left|\left|\boldsymbol{v}\right|\right|\right|_{r,p} := \left(\Delta t \sum_{n=1}^{N} \left|\left|\boldsymbol{v}^n\right|\right|_p^r\right)^{\frac{1}{r}}, \quad \left|\left|\left|\boldsymbol{v}\right|\right|\right|_{\infty,p} := max_{\ 0\leq n\leq N} \left|\left|\boldsymbol{v}^n\right|\right|_p,$$

where Δt denotes the time step, the variables at time $t^n,\ n = 1,2,\dots,N$ are given using superscripts, e.g. $\boldsymbol{v}^n = \boldsymbol{v}(t^n)$. A conforming finite element method is considered for (2) such that T_h is a triangulation with mesh size h. The finite element spaces $\boldsymbol{X}_h \subset \boldsymbol{X}, Q_h \subset Q$ satisfy the discrete inf-sup condition. Moreover, $\boldsymbol{X}_h, Q_h$ are composed of piecewise polynomials of degree at most $s,\ s-1$, respectively, and they satisfy the following approximation properties:

$$\inf_{\mathbf{w}_h\in\mathbf{X}_\mathrm{h}} \left\{\left|\left|\boldsymbol{u}-\boldsymbol{w}_h\right|\right|^2\right\} \leq\ C\ h^{2s+2}\left|\left|\boldsymbol{u}\right|\right|_{s+1}^2,$$

$$\inf_{\mathbf{w}_h\in\mathbf{X}_\mathrm{h}} \left\{\left|\left|\nabla(\boldsymbol{u}-\boldsymbol{w}_h)\right|\right|^2\right\} \leq\ C\ h^{2s}\left|\left|\boldsymbol{u}\right|\right|_{s+1}^2,$$

$$\inf_{\mathrm{q}_h\in\mathrm{Q}_\mathrm{h}} \left\{\left|\left|p-q_h\right|\right|^2\right\} \leq\ C\ h^{2s}\left|\left|p\right|\right|_s^2 \tag{3}$$

where $\boldsymbol{u} \in\ \boldsymbol{H}^{s+1}(\Omega), p \in\ H^s(\Omega)$. The discretely divergence free space is given by

$$\boldsymbol{V}_h = \{\boldsymbol{v}_h \in\ \boldsymbol{X}_h\colon (\nabla\cdot\ \boldsymbol{v}_h, q_h) = 0, \forall q_h \in\ Q_h\}\ .$$

As $\boldsymbol{V}_h$ is a closed subspace of $\boldsymbol{X}_h$, the formulation (3) is equivalent to the following $\boldsymbol{V}_h$ formulation:

$$\left(\boldsymbol{u}_{h,t}, \boldsymbol{v}_h\right) + \nu(\nabla\boldsymbol{u}_h\ , \nabla\boldsymbol{v}_h) +\ b(\boldsymbol{u}_h, \boldsymbol{u}_h, \boldsymbol{v}_h) = (\ \boldsymbol{f}, \boldsymbol{v}_h),$$

for all $\boldsymbol{v}_h \in\ \boldsymbol{V}_h$. Let $D = span\{\boldsymbol{u}(\cdot,t_1), \boldsymbol{u}(\cdot,t_2), \dots, \boldsymbol{u}(\cdot,t_N)\}$ be a snapshots ensemble for given time instances $t_k = k\Delta t, k = 1,\dots,N$, for $N = \frac{\tau}{\Delta \mathrm{t}}$. To find low dimensional POD basis functions, the following error minimization problem is solved.

$$\underset{\boldsymbol{\psi}_1,\boldsymbol{\psi}_2,\dots,\boldsymbol{\psi}_r}{\arg\min} \frac{1}{N}\sum_{k=1}^{N}\left|\left|\boldsymbol{u}(\cdot,t_k) - \sum_{j=1}^{r}\left(\boldsymbol{u}(\cdot,t_k), \boldsymbol{\psi}_j(\cdot)\right)\boldsymbol{\psi}_j(\cdot)\right|\right|^2,$$

such that $\left(\boldsymbol{\psi}_i, \boldsymbol{\psi}_j\right) = \delta_{ij}, 1 \leq\ i,j \leq\ r,\ r << d$ and $d = rank(D)$. Using properties of inner products and norms, an eigenvalue problem,

$$Z\boldsymbol{\gamma_j} = \mu\boldsymbol{\gamma_j}\ , j = 1,\dots,r$$

is obtained. Here $Z \in \mathbb{R}^{N\times N}$ with $Z_{ki} = \frac{1}{N}\left(\boldsymbol{u}(\cdot,t_i), \boldsymbol{u}(\cdot,t_k)\right),\ \ i,k = 1,\dots,N$, is the snapshots correlation matrix, μ_j is the j-th eigenvalue, and $\boldsymbol{\gamma}_j$ is the associated eigenvector. The solution of the eigenvalue problem produces POD basis functions $\{\boldsymbol{\psi}_1, \boldsymbol{\psi}_2, \dots, \boldsymbol{\psi}_r\}$ corresponding to the first r largest eigenvalues $\{\mu_i\}_{i=1}^r$, respectively. Accordingly, the POD space is defined by

$$\boldsymbol{X}_r\ =\ span\{\boldsymbol{\psi}_1, \boldsymbol{\psi}_2, \dots, \boldsymbol{\psi}_r\}.$$

In the VMS-POD setting, the POD space $\boldsymbol{X}_r$ is decomposed to small resolved scale space $\boldsymbol{X}_S = span\{\boldsymbol{\psi}_{R+1}, \boldsymbol{\psi}_{R+2}, \dots, \boldsymbol{\psi}_r\}$ and large resolved scale space $\boldsymbol{X}_R = span\{\boldsymbol{\psi}_1, \boldsymbol{\psi}_2, \dots \boldsymbol{\psi}_R\}$, with $R < r$. We also need the space $\boldsymbol{L}_{R,\boldsymbol{u}} = \nabla \boldsymbol{X}_R = span\{\nabla\boldsymbol{\psi}_1, \nabla\boldsymbol{\psi}_2, \dots \nabla\boldsymbol{\psi}_R\}$, to define the projection operator. Note that, one gets $\boldsymbol{X}_R \subseteq \boldsymbol{X}_r \subset \boldsymbol{X}_h \subset \boldsymbol{X}$. The L^2 projection operators $P_{\boldsymbol{u},r}: L^2 \to \boldsymbol{X}_r$, and $P_{\boldsymbol{u},R}: L^2 \to \boldsymbol{L}_{R,\boldsymbol{u}}$ are denoted by

$$\left(\boldsymbol{u} - P_{\boldsymbol{u},r}\boldsymbol{u}, \boldsymbol{v}_r\right) = 0, \quad \forall\ \boldsymbol{v}_r \in \boldsymbol{X}_r,$$

$$\left(\boldsymbol{u} - P_{\boldsymbol{u},R}\boldsymbol{u}, \boldsymbol{v}_R\right) = 0, \ \forall\ \boldsymbol{v}_R \in \boldsymbol{L}_{R,\boldsymbol{u}}.$$

The following lemma is required to bound the POD projection error.

Lemma 2.2. For the true solution $\boldsymbol{u}^n$ at time t^n, we have

$$\frac{1}{M}\sum_{n=1}^{N}\left|\left|\boldsymbol{u}^n - P_{\boldsymbol{u},r}\boldsymbol{u}^n\right|\right|^2 \le C\left(h^{2s+2}\left|\left|\boldsymbol{u}\right|\right|^2_{2,s+1} + \sum_{i=r+1}^{d}\mu_i\right),$$

$$\frac{1}{M}\sum_{n=1}^{N}\left|\left|\nabla(\boldsymbol{u}^n - P_{\boldsymbol{u},r}\boldsymbol{u}^n)\right|\right|^2 \le C\left(\left(h^{2s} + \left|\left|\mathcal{S}_r\right|\right|_2 h^{2s+2}\right)\left|\left|\boldsymbol{u}\right|\right|^2_{2,s+1} + \sum_{i=r+1}^{d}\left|\left|\boldsymbol{\psi}_i\right|\right|_1^2\mu_i\right),$$

where $\mathcal{S}_r$ denotes the POD stiffness matrix with $(\mathcal{S}_r)_{ij} = \int_\Omega \nabla\boldsymbol{\psi}_i \cdot \nabla\boldsymbol{\psi}_j\, d\boldsymbol{x}$.

Proof. Please see [6] for the proof.

Assumption 2.1. We assume that the following inequalities hold

$$\left|\left|\boldsymbol{u}^n - P_{\boldsymbol{u},r}\boldsymbol{u}^n\right|\right|^2 \le C\left(h^{2s+2}\left|\left|\boldsymbol{u}\right|\right|^2_{2,s+1} + \sum_{i=r+1}^{d}\mu_i\right),$$

$$\left|\left|\nabla(\boldsymbol{u}^n - P_{\boldsymbol{u},r}\boldsymbol{u}^n)\right|\right|^2 \le C\left(\left(h^{2s} + \left|\left|\mathcal{S}_r\right|\right|_2 h^{2s+2}\right)\left|\left|\boldsymbol{u}\right|\right|^2_{2,s+1} + \sum_{i=r+1}^{d}\left|\left|\boldsymbol{\psi}_i\right|\right|_1^2\mu_i\right).$$

2.1. The Time Filtered VMS-POD Schemes

This section introduces the time filtered backward Euler based VMS-POD method for NSE. At each time step, there is a two-step procedure: The first step develops the VMS-POD approximate solution based on backward Euler time discretization, and then the second step evolves this solution using the linear combination of solutions at previous time levels.

Algorithm 2.1. Let $\boldsymbol{f} \in L^2\left(0,\tau;\boldsymbol{H}^{-1}(\Omega)\right)$, $\boldsymbol{u}_r^0$ and $\boldsymbol{u}_r^{-1}$ be given with L^2 projections of initial condition $\boldsymbol{u}_0$ in $\boldsymbol{X}_r$. Given $\boldsymbol{u}_r^n, \boldsymbol{u}_r^{n-1} \in \boldsymbol{X}_r$, compute $\boldsymbol{u}_r^{n+1}$ for $n = 0, 1, \dots, N-1$ by applying the following two steps:

Step 1:

$$\left(\frac{\widetilde{\boldsymbol{u}_r}^{n+1} - \boldsymbol{u}_r^n}{\Delta t}, \boldsymbol{v}_r\right) + \nu\left(\nabla\widetilde{\boldsymbol{u}_r}^{n+1}, \nabla\,\boldsymbol{v}_r\right) + b\left(\mathcal{X}(\boldsymbol{u}_r^n), \widetilde{\boldsymbol{u}_r}^{n+1}, \boldsymbol{v}_r\right) + \nu_T\left(\widetilde{P}_{\boldsymbol{u},R}\nabla\,\widetilde{\boldsymbol{u}_r}^{n+1}, \widetilde{P}_{\boldsymbol{u},R}\nabla\ \boldsymbol{v}_r\right)$$
$$= (\boldsymbol{f}, \boldsymbol{v}_r). \tag{4}$$

Step 2:

$$\boldsymbol{u}_r^{n+1} = \widetilde{\boldsymbol{u}_r}^{n+1} - \frac{1}{3}\left(\widetilde{\boldsymbol{u}_r}^{n+1} - 2\boldsymbol{u}_r^n + \boldsymbol{u}_r^{n-1}\right), \tag{5}$$

for all $\boldsymbol{v}_r \in \boldsymbol{X}_r$. Here $\mathcal{X}(\boldsymbol{u}_r^n) = 2\boldsymbol{u}_r^n - \boldsymbol{u}_r^{n-1}$ and $\widetilde{P}_{\boldsymbol{u},R} = I - P_{\boldsymbol{u},R}$. Reorganizing Step 2, we have

$$\widetilde{\boldsymbol{u}}_r^{n+1} = \frac{3}{2}\boldsymbol{u}_r^{n+1} - \boldsymbol{u}_r^n + \frac{1}{2}\boldsymbol{u}_r^{n-1} = \mathcal{D}[\boldsymbol{u}_r^{n+1}] \tag{6}$$

where the interpolation operator $\mathcal{D}$ satisfies $\mathcal{D}[\boldsymbol{u}_r^{n+1}] = \boldsymbol{u}_r^{n+1} + \mathcal{O}(\Delta t^2)$. Inserting (6) in (4) produces: Find $\boldsymbol{u}_r^{n+1} \in \boldsymbol{X}_r$ satisfying

$$\left(\frac{3\boldsymbol{u}_r^{n+1} - 4\boldsymbol{u}_r^n + \boldsymbol{u}_r^{n-1}}{2\Delta t}, \boldsymbol{v}_r\right) + \nu(\nabla\mathcal{D}[\boldsymbol{u}_r^{n+1}], \nabla\boldsymbol{v}_r) + b(\mathcal{X}(\boldsymbol{u}_r^n), \mathcal{D}[\boldsymbol{u}_r^{n+1}], \boldsymbol{v}_r)$$

$$+\nu_T\left(\widetilde{P}_{u,R}\nabla\mathcal{D}[\boldsymbol{u}_r^{n+1}], \widetilde{P}_{u,R}\nabla\boldsymbol{v}_r\right) = (\boldsymbol{f}^{n+1}, \boldsymbol{v}_r), \tag{7}$$

for all $\boldsymbol{v}_r \in \boldsymbol{X}_r$. It is clear that (7) is equivalent to Algorithm 2.1. Even though the temporal discretization of the first term on the left-hand side seems two-step BDF-method (BDF2), the remaining parts of the equation are different. Hence, the proposed method is not the same as standard BDF2. To simplify the analysis, the G-stability concept is utilized as in [16, 17] with the following definitions of symmetric G-matrix and G-norm:

$$G = \frac{1}{4}\begin{pmatrix} 6 & -3 \\ -3 & 2 \end{pmatrix}, \quad \left|\left|\mathcal{U}\right|\right|_G^2 = (\mathcal{U}, G\mathcal{U}), \ \ \forall\mathcal{U} \in \mathbb{R}^{2n}. \tag{8}$$

In addition, let $F = 3I \in \mathbb{R}^{n\times n}$ be a positive, symmetric matrix, and $\forall w \in \mathbb{R}^n$, then F-norm of w can be expressed as $||w||_F^2 = (w, Fw)$. The Lemmas below are well known and essential in the analysis. For a detailed derivation of these relations, please see [16, 17].

Lemma 2.3. For any $w^i \in L^2(\Omega)$, we have

$$\left(\frac{3w^{n+1} - 4w^n + w^{n-1}}{2\Delta t}, \mathcal{D}[w^{n+1}]\right) = \frac{1}{\Delta t}\left(\left\|\begin{bmatrix} w^{n+1} \\ w^n \end{bmatrix}\right\|_G^2 - \left\|\begin{bmatrix} w^n \\ w^{n-1} \end{bmatrix}\right\|_G^2 + \frac{1}{4}\left|\left|w^{n+1} - 2w^n + w^{n-1}\right|\right|_F^2\right).$$

Lemma 2.4. Let $w_1, w_2 \in L^2(\Omega)$, then we get

$$\left(\begin{bmatrix} w_1 \\ w_2 \end{bmatrix}, G\begin{bmatrix} w_1 \\ w_2 \end{bmatrix}\right) = \frac{1}{4}\left(\left|\left|w_1\right|\right|^2 + \left|\left|2w_1 - w_2\right|\right|^2 + \left|\left|w_1 - w_2\right|\right|^2\right).$$

Lemma 2.5. The equivalence relation between L^2 norm and G-norm is given by the following inequality. There exists $\mathcal{C}_1,\ \mathcal{C}_2 > 0$ such that

$$\mathcal{C}_1\left\|\begin{bmatrix} w_1 \\ w_2 \end{bmatrix}\right\|_G^2 \le \left\|\begin{bmatrix} w_1 \\ w_2 \end{bmatrix}\right\|^2 \le \mathcal{C}_2\left\|\begin{bmatrix} w_1 \\ w_2 \end{bmatrix}\right\|_G^2.$$

Lemma 2.6. Let $w, w_t, w_{tt}, w_{ttt} \in L^2(t^n, t^{n+1}; L^2(\Omega))$, then we have the following inequalities

$$\Delta t\sum_{n=0}^{N-1}\left|\left|\mathcal{D}[w^{n+1}] - w^{n+1}\right|\right|^2 \le C\Delta t^4\left|\left|w_{tt}\right|\right|_{L^2\left(0,T;L^2(\Omega)\right)}^2,$$

$$\Delta t \sum_{n=0}^{N-1} \left|\left|\mathcal{X}(w^n) - w^{n+1}\right|\right|^2 \leq C\Delta t^4 \left|\left|w_{tt}\right|\right|^2_{L^2\left(0,T;L^2(\Omega)\right)},$$

$$\Delta t \sum_{n=0}^{N-1} \left|\left|\frac{3w^{n+1} - 4w^n + w^{n-1}}{2\Delta t} - w_t^{n+1}\right|\right|^2 \leq C\Delta t^4 \left|\left|w_{ttt}\right|\right|^2_{L^2\left(0,T;L^2(\Omega)\right)}.$$

Lemma 2.7. (Discrete Gronwall) Let $a_n, b_n, c_n, \delta_n, \Delta t$ and K be nonnegative numbers for $n \geq 0$ and

$$a_N + \Delta t \sum_{n=0}^{N} b_n \leq \Delta t \sum_{n=0}^{N} \delta_n a_n + \Delta t \sum_{n=0}^{N} c_n + K, \;\; N \geq 0 \tag{9}$$

then if $\Delta t \delta_n < 1$ for all n, we get

$$a_N + \Delta t \sum_{n=0}^{N} b_n \leq \exp\left(\Delta t \sum_{n=0}^{N} \frac{\delta_n}{1 - \Delta t \delta_n}\right)\left(\Delta t \sum_{n=0}^{N} c_n + K\right), \;\; N \geq 0. \tag{10}$$

Proof. Please see [19] for the proof.

Lemma 2.8. Let $v \in H^1(\Omega)$. Then the following inequality holds.

$$\left|\left|\nabla \cdot v\right|\right| \leq \sqrt{d}\left|\left|\nabla v\right|\right|$$

where d denotes the dimension of the domain Ω.

3. NUMERICAL ANALYSIS OF THE NAVIER-STOKES SYSTEM

The goal of this section is to show that our scheme (7) is energy preserving and unconditionally stable. We also present the convergence analysis of the method.

Lemma 3.1. (Global Energy Conservation) The approximation (7) satisfies the energy equality:

$$\left|\left|\left|\begin{bmatrix} \boldsymbol{u}_r^N \\ \boldsymbol{u}_r^{N-1} \end{bmatrix}\right|\right|\right|_G^2 + \frac{1}{4}\sum_{n=0}^{N-1} \left|\left|\boldsymbol{u}_r^{n+1} - 2\boldsymbol{u}_r^n + \boldsymbol{u}_r^{n-1}\right|\right|_F^2 + \Delta t \sum_{n=0}^{N-1} \left(\nu \left|\left|\nabla \mathcal{D}[\boldsymbol{u}_r^{n+1}]\right|\right|^2 + \nu_T \left|\left|\widetilde{P}_{\boldsymbol{u},R} \nabla \mathcal{D}[\boldsymbol{u}_r^{n+1}]\right|\right|^2\right)$$

$$= \left|\left|\left|\begin{bmatrix} \boldsymbol{u}_r^0 \\ \boldsymbol{u}_r^{-1} \end{bmatrix}\right|\right|\right|_G^2 + \Delta t \sum_{n=0}^{N-1} (\boldsymbol{f}^{n+1}, \mathcal{D}[\boldsymbol{u}_r^{n+1}]). \tag{11}$$

Proof. Letting $\boldsymbol{v}_r = \mathcal{D}[\boldsymbol{u}_r^{n+1}]$, using Lemma 2.3 and the skew symmetry property in (7) yields

$$\frac{1}{\Delta t}\left|\left|\left|\begin{bmatrix} \boldsymbol{u}_r^{n+1} \\ \boldsymbol{u}_r^n \end{bmatrix}\right|\right|\right|_G^2 - \frac{1}{\Delta t}\left|\left|\left|\begin{bmatrix} \boldsymbol{u}_r^n \\ \boldsymbol{u}_r^{n-1} \end{bmatrix}\right|\right|\right|_G^2 + \frac{1}{4\Delta \mathrm{t}}\left|\left|\boldsymbol{u}_r^{n+1} - 2\boldsymbol{u}_r^n + \boldsymbol{u}_r^{n-1}\right|\right|_F^2$$

$$+\nu\left|\left|\nabla \mathcal{D}[\boldsymbol{u}_r^{n+1}]\right|\right|^2 + \nu_T \left|\left|\widetilde{P}_{\boldsymbol{u},R} \nabla \mathcal{D}[\boldsymbol{u}_r^{n+1}]\right|\right|^2 = (\boldsymbol{f}^{n+1}, \mathcal{D}[\boldsymbol{u}_r^{n+1}]). \tag{12}$$

Summing over the time steps and multiplying by Δt yields the energy equality (11).

Lemma 3.2. (Stability) Assume $\boldsymbol{f} \in L^2(0,\tau;\boldsymbol{H}^{-1}(\Omega))$, then the approximation (7) is unconditionally stable in the following sense: for any $\Delta t > 0$,

$$\left||\boldsymbol{u}_r^N|\right|^2 + \left||2\boldsymbol{u}_r^N - \boldsymbol{u}_r^{N-1}|\right|^2 + \left||\boldsymbol{u}_r^N - \boldsymbol{u}_r^{N-1}|\right|^2 + \sum_{n=0}^{N-1}\left||\boldsymbol{u}_r^{n+1} - 2\boldsymbol{u}_r^n + \boldsymbol{u}_r^{n-1}|\right|_F^2$$

$$+\Delta t\sum_{n=0}^{N-1}\left(2\nu\left||\nabla\mathcal{D}[\boldsymbol{u}_r^{n+1}]|\right|^2 + 4\nu_T\left|\left|\widetilde{P}_{\boldsymbol{u},R}\nabla\mathcal{D}[\boldsymbol{u}_r^{n+1}]\right|\right|^2\right)$$

$$\leq \left||\boldsymbol{u}_r^0|\right|^2 + \left||2\boldsymbol{u}_r^0 - \boldsymbol{u}_r^{-1}|\right|^2 + \left||\boldsymbol{u}_r^0 - \boldsymbol{u}_r^{-1}|\right|^2 + 2\nu^{-1}\Delta t\sum_{n=0}^{N-1}\left||\boldsymbol{f}^{n+1}|\right|_{-1}^2. \tag{13}$$

Proof. Applying Cauchy-Schwarz inequality together with Young's inequality to the right-hand side of (12) gives

$$\Delta t\,(\,\boldsymbol{f}^{n+1},\mathcal{D}[\boldsymbol{u}_r^{n+1}]) \leq \frac{\nu^{-1}\,\Delta t}{2}\left||\boldsymbol{f}^{n+1}|\right|_{-1}^2 + \frac{\nu\,\Delta t}{2}\left||\nabla\mathcal{D}[\boldsymbol{u}_r^{n+1}]|\right|^2. \tag{14}$$

Substituting (14) in (12), utilizing Lemma 2.4, summing over the time steps and multiplying by 4 produces the stated result (13).

The following regularity assumptions of the exact solution are needed for the optimal error estimation:

$$\begin{aligned}&\boldsymbol{u} \in L^\infty\big(0,\tau;\ \boldsymbol{H}^{s+1}(\Omega)\big),\quad \boldsymbol{u}_{tt} \in L^2\big(0,\tau;\boldsymbol{H}^1(\Omega)\big),\qquad \boldsymbol{u}_{ttt} \in L^2\big(0,\tau;L^2(\Omega)\big),\\ &p \in L^\infty\big(0,\tau;H^s(\Omega)\big),\quad \boldsymbol{f} \in L^2\big(0,\tau;\boldsymbol{H}^{-1}(\Omega)\big).\end{aligned} \tag{15}$$

Theorem 3.1. (Error estimation) Let regularity assumptions (15) hold. For a sufficiently small time-step, the error satisfies

$$||\boldsymbol{u}^N - \boldsymbol{u}_r^N||^2 + 2\Delta t\sum_{n=0}^{N-1}\left(\nu\left||\nabla\mathcal{D}[\boldsymbol{u}^{n+1} - \boldsymbol{u}_r^{n+1}]|\right|^2 + \nu_T\left|\left|\widetilde{P}_{\boldsymbol{u},R}\nabla\mathcal{D}[\boldsymbol{u}^{n+1} - \boldsymbol{u}_r^{n+1}]\right|\right|^2\right)$$

$$\leq ||\boldsymbol{u}^0 - \boldsymbol{u}_r{}^0||^2 + ||2(\boldsymbol{u}^0 - \boldsymbol{u}_r{}^0) - (\boldsymbol{u}^{-1} - \boldsymbol{u}_r{}^{-1})||^2 + ||(\boldsymbol{u}^0 - \boldsymbol{u}_r{}^0) - (\boldsymbol{u}^{-1} - \boldsymbol{u}_r{}^{-1})||^2$$

$$+C^*\left(1 + h^{2s} + \Delta t^4 + \left(1 + \left|\left|\mathcal{S}_r\right|\right|_2 + \left|\left|\mathcal{S}_R\right|\right|_2\right)h^{2s+2} + \sum_{i=r+1}^{d}\left(1 + \left||\boldsymbol{\psi}_i|\right|_1^2\right)\mu_i + \sum_{i=R+1}^{d}\left||\boldsymbol{\psi}_i|\right|_1^2\mu_i\right) \tag{16}$$

where C^* is a generic constant independent of Δt and h.

Proof. To derive the error equations, the continuous variational formulation of (1) at the time level $t = t^{n+1}$ is considered. Adding and subtracting the terms produces, for all $\boldsymbol{v}_r \in \boldsymbol{X}_r$

$$\left(\frac{3\boldsymbol{u}^{n+1} - 4\boldsymbol{u}^n + \boldsymbol{u}^{n-1}}{2\Delta t}, \boldsymbol{v}_r\right) + \nu(\nabla\mathcal{D}[\boldsymbol{u}^{n+1}], \nabla\,\boldsymbol{v}_r) + b(\mathcal{X}(\boldsymbol{u}^n), \mathcal{D}[\boldsymbol{u}^{n+1}], \boldsymbol{v}_r)$$

$$+\nu_T\big(\widetilde{P}_{\boldsymbol{u},R}\nabla\mathcal{D}[\boldsymbol{u}^{n+1}],\ \widetilde{P}_{\boldsymbol{u},R}\nabla\boldsymbol{v}_r\big) - (\,p^{n+1}, \nabla\cdot\boldsymbol{v}_r) = (\,\boldsymbol{f}(t^{n+1}), \boldsymbol{v}_r) + E(\boldsymbol{u}, \boldsymbol{v}_r) \tag{17}$$

where

$$E(\boldsymbol{u},\boldsymbol{v_r})=\left(\frac{3\boldsymbol{u}^{n+1}-4\boldsymbol{u}^{n}+\boldsymbol{u}^{n-1}}{2\Delta t}-\boldsymbol{u}_t^{n+1},\boldsymbol{v}_r\right)+\nu(\nabla\mathcal{D}[\boldsymbol{u}^{n+1}],\nabla\boldsymbol{v}_r)-\nu(\nabla\boldsymbol{u}^{n+1},\nabla\boldsymbol{v}_r)$$

$$+\nu_T\big(\widetilde{P}_{\boldsymbol{u},R}\nabla\mathcal{D}[\boldsymbol{u}^{n+1}],\widetilde{P}_{\boldsymbol{u},R}\nabla\boldsymbol{v}_r\big)+b(\mathcal{X}(\boldsymbol{u}^{n}),\mathcal{D}[\boldsymbol{u}^{n+1}],\boldsymbol{v}_r)-b(\boldsymbol{u}^{n+1},\boldsymbol{u}^{n+1},\boldsymbol{v}_r).$$

Subtracting (7) from (17) gives, $\forall\boldsymbol{v}_r\in\boldsymbol{X}_r$ and $\forall q_h\in Q_h$

$$\left(\frac{3\boldsymbol{e}_r^{n+1}-4\boldsymbol{e}_r^{n}+\boldsymbol{e}_r^{n-1}}{2\Delta t},\boldsymbol{v}_r\right)+\nu(\nabla\mathcal{D}[\boldsymbol{e}_r^{n+1}],\nabla\boldsymbol{v}_r)+b(\mathcal{X}(\boldsymbol{u}_r^{n}),\mathcal{D}[\boldsymbol{e}_r^{n+1}],\boldsymbol{v}_r)$$

$$+b(\mathcal{X}(\boldsymbol{e}_r^{n}),\mathcal{D}[\boldsymbol{u}^{n+1}],\boldsymbol{v}_r)+\nu_T\big(\widetilde{P}_{\boldsymbol{u},R}\nabla\mathcal{D}[\boldsymbol{e}_r^{n+1}],\widetilde{P}_{\boldsymbol{u},R}\nabla\boldsymbol{v}_r\big)-(p^{n+1}-q_h,\nabla\cdot\boldsymbol{v}_r)=E(\boldsymbol{u},\boldsymbol{v_r}) \tag{18}$$

where $\boldsymbol{e}_r^{n+1}=\boldsymbol{u}^{n+1}-\boldsymbol{u}_r^{n+1}$ is the error between the continuous and finite element solutions at the time level $t=t^{n+1}$. The error can be decomposed as

$$\boldsymbol{e}_r^{n+1}=\boldsymbol{u}^{n+1}-\boldsymbol{u}_r^{n+1}=(\boldsymbol{u}^{n+1}-\mathcal{U}^{n+1})-(\boldsymbol{u}_r^{n+1}-\mathcal{U}^{n+1})=\boldsymbol{\eta}^{n+1}-\boldsymbol{\phi}_r^{n+1} \tag{19}$$

where $\mathcal{U}^{n+1}$ is the L^2 projection of $\boldsymbol{u}^{n+1}$ in $\boldsymbol{X}_r$. Inserting (19) into (18), setting $\boldsymbol{v_r}=\mathcal{D}[\boldsymbol{\phi}_r^{n+1}]$, using Lemma 2.3 and the skew symmetry property give

$$\frac{1}{\Delta t}\left\|\begin{bmatrix}\boldsymbol{\phi}_r^{n+1}\\ \boldsymbol{\phi}_r^{n}\end{bmatrix}\right\|_G^2-\frac{1}{\Delta t}\left\|\begin{bmatrix}\boldsymbol{\phi}_r^{n}\\ \boldsymbol{\phi}_r^{n-1}\end{bmatrix}\right\|_G^2+\frac{1}{4\Delta\mathrm{t}}\big||\boldsymbol{\phi}_r^{n+1}-2\boldsymbol{\phi}_r^{n}+\boldsymbol{\phi}_r^{n-1}|\big|_F^2$$

$$+\nu\big||\nabla\mathcal{D}[\boldsymbol{\phi}_r^{n+1}]|\big|^2+\nu_T\left|\left|\widetilde{P}_{\boldsymbol{u},R}\nabla\mathcal{D}[\boldsymbol{\phi}_r^{n+1}]\right|\right|^2$$

$$\leq\left|\left(\frac{3\boldsymbol{\eta}^{n+1}-4\boldsymbol{\eta}^{n}+\boldsymbol{\eta}^{n-1}}{2\Delta t},\boldsymbol{\phi}_r^{n+1}\right)\right|+\nu|(\nabla\mathcal{D}[\boldsymbol{\eta}^{n+1}],\nabla\mathcal{D}[\boldsymbol{\phi}_r^{n+1}])|$$

$$+\nu_T\big|\big(\widetilde{P}_{\boldsymbol{u},R}\nabla\mathcal{D}[\boldsymbol{\eta}^{n+1}],\widetilde{P}_{\boldsymbol{u},R}\nabla\mathcal{D}[\boldsymbol{\phi}_r^{n+1}]\big)\big|+|b(\mathcal{X}(\boldsymbol{u}_r^{n}),\mathcal{D}[\boldsymbol{\eta}^{n+1}],\mathcal{D}[\boldsymbol{\phi}_r^{n+1}])|$$

$$+|b(\mathcal{X}(\boldsymbol{\eta}^{n}),\mathcal{D}[\boldsymbol{u}^{n+1}],\mathcal{D}[\boldsymbol{\phi}_r^{n+1}])|+|b(\mathcal{X}(\boldsymbol{\phi}_r^{n}),\mathcal{D}[\boldsymbol{u}^{n+1}],\mathcal{D}[\boldsymbol{\phi}_r^{n+1}])|$$

$$|(p^{n+1}-q_h,\nabla\cdot\mathcal{D}[\boldsymbol{\phi}_r^{n+1}])|+|E(\boldsymbol{u},\mathcal{D}[\boldsymbol{\phi}_r^{n+1}])|. \tag{20}$$

Due to the definition of L^2 projection, the first right-hand side term in (20) vanishes. Implementing Cauchy-Schwarz and Young's inequalities and using $\left|\left|\widetilde{P}_{\boldsymbol{u},R}\nabla\mathcal{D}[\boldsymbol{\eta}^{n+1}]\right|\right|^2\leq\big||\nabla\mathcal{D}[\boldsymbol{\eta}^{n+1}]|\big|^2$, the second and third terms on the right-hand side of (20) are estimated as follows:

$$\nu|(\nabla\mathcal{D}[\boldsymbol{\eta}^{n+1}],\nabla\mathcal{D}[\boldsymbol{\phi}_r^{n+1}])|\leq C\nu\big||\nabla\mathcal{D}[\boldsymbol{\eta}^{n+1}]|\big|^2+\frac{\nu}{12}\big||\nabla\mathcal{D}[\boldsymbol{\phi}_r^{n+1}]|\big|^2, \tag{21}$$

$$\nu_T\big|\big(\widetilde{P}_{\boldsymbol{u},R}\nabla\mathcal{D}[\boldsymbol{\eta}^{n+1}],\widetilde{P}_{\boldsymbol{u},R}\nabla\mathcal{D}[\boldsymbol{\phi}_r^{n+1}]\big)\big|\leq C\nu_T\big||\nabla\mathcal{D}[\boldsymbol{\eta}^{n+1}]|\big|^2+\frac{\nu_T}{4}\left|\left|\widetilde{P}_{\boldsymbol{u},R}\nabla\mathcal{D}[\boldsymbol{\phi}_r^{n+1}]\right|\right|^2. \tag{22}$$

The nonlinear terms are bounded by using Lemma 2.1 and Young's inequality as

$$|b(\mathcal{X}(\boldsymbol{u}_r^{n}),\mathcal{D}[\boldsymbol{\eta}^{n+1}],\mathcal{D}[\boldsymbol{\phi}_r^{n+1}])|+|b(\mathcal{X}(\boldsymbol{\eta}^{n}),\mathcal{D}[\boldsymbol{u}^{n+1}],\mathcal{D}[\boldsymbol{\phi}_r^{n+1}])|+|b(\mathcal{X}(\boldsymbol{\phi}_r^{n}),\mathcal{D}[\boldsymbol{u}^{n+1}],\mathcal{D}[\boldsymbol{\phi}_r^{n+1}])|$$
$$\leq C\nu^{-1}\big(\big||\nabla\mathcal{X}(\boldsymbol{u}_r^{n})|\big|^2\big||\nabla\mathcal{D}[\boldsymbol{\eta}^{n+1}]|\big|^2+\big||\nabla\mathcal{X}(\boldsymbol{\eta}^{n})|\big|^2\big||\nabla\mathcal{D}[\boldsymbol{u}^{n+1}]|\big|^2$$

$$+\big||\nabla\mathcal{X}(\boldsymbol{\phi}_r^{n})|\big|^2\big||\nabla\mathcal{D}[\boldsymbol{u}^{n+1}]|\big|^2\big)+\frac{\nu}{12}\big||\nabla\mathcal{D}[\boldsymbol{\phi}_r^{n+1}]|\big|^2. \tag{23}$$

Now, the consistency error $|E(\boldsymbol{u}, \mathcal{D}[\boldsymbol{\phi}_r^{n+1}])|$ in (20) can be bounded by using Cauchy-Schwarz, Young's and Poincaré's inequalities together with Lemma 2.1:

$$\left|\left(\frac{3\boldsymbol{u}^{n+1}-4\boldsymbol{u}^{n}+\boldsymbol{u}^{n-1}}{2\Delta t}-\boldsymbol{u}_t^{n+1}, \mathcal{D}[\boldsymbol{\phi}_r^{n+1}]\right)\right|$$

$$\leq C\nu^{-1}\left|\left|\frac{3\boldsymbol{u}^{n+1}-4\boldsymbol{u}^{n}+\boldsymbol{u}^{n-1}}{2\Delta t}-\boldsymbol{u}_t^{n+1}\right|\right|^2+\frac{\nu}{12}\left||\nabla\mathcal{D}[\boldsymbol{\phi}_r^{n+1}]|\right|^2, \tag{24}$$

$$\nu|(\nabla(\mathcal{D}[\boldsymbol{u}^{n+1}]-\boldsymbol{u}^{n+1}), \nabla\mathcal{D}[\boldsymbol{\phi}_r^{n+1}])| \leq C\nu\left||\nabla(\mathcal{D}[\boldsymbol{u}^{n+1}]-\boldsymbol{u}^{n+1})|\right|^2+\frac{\nu}{12}\left||\nabla\mathcal{D}[\boldsymbol{\phi}_r^{n+1}]|\right|^2, \tag{25}$$

$$\nu_T\left|\left(\widetilde{P}_{\boldsymbol{u},R}\nabla\mathcal{D}[\boldsymbol{u}^{n+1}], \widetilde{P}_{\boldsymbol{u},R}\nabla\mathcal{D}[\boldsymbol{\phi}_r^{n+1}]\right)\right| \leq C\nu_T\left|\left|\widetilde{P}_{\boldsymbol{u},R}\nabla\mathcal{D}[\boldsymbol{u}^{n+1}]\right|\right|^2+\frac{\nu_T}{4}\left||\nabla\mathcal{D}[\boldsymbol{\phi}_r^{n+1}]|\right|^2, \tag{26}$$

$$b(\mathcal{X}(\boldsymbol{u}^n), \mathcal{D}[\boldsymbol{u}^{n+1}], \mathcal{D}[\boldsymbol{\phi}_r^{n+1}]) - b(\boldsymbol{u}^{n+1}, \boldsymbol{u}^{n+1}, \mathcal{D}[\boldsymbol{\phi}_r^{n+1}])$$

$$\leq C\nu^{-1}\left(\left||\nabla\mathcal{X}(\boldsymbol{u}^n)|\right|^2\left||\nabla(\mathcal{D}[\boldsymbol{u}^{n+1}]-\boldsymbol{u}^{n+1})|\right|^2+\left||\nabla(\mathcal{X}(\boldsymbol{u}^n)-\boldsymbol{u}^{n+1})|\right|^2\left||\nabla\boldsymbol{u}^{n+1}|\right|^2\right)$$

$$+\frac{\nu}{12}\left||\nabla\mathcal{D}[\boldsymbol{\phi}_r^{n+1}]|\right|^2. \tag{27}$$

Using Cauchy-Schwarz and Young's inequalities together with Lemma 2.8, the pressure term is estimated by

$$|(p^{n+1}-q_h, \nabla\cdot\mathcal{D}[\boldsymbol{\phi}_r^{n+1}])| \leq \inf_{q\in Q_h}\left||p^{n+1}-q_h|\right|\left||\nabla\cdot\mathcal{D}[\boldsymbol{\phi}_r^{n+1}]|\right|$$

$$\leq \sqrt{d}\inf_{q\in Q_h}\left||p^{n+1}-q_h|\right|\left||\nabla\mathcal{D}[\boldsymbol{\phi}_r^{n+1}]|\right|$$

$$\leq C\nu^{-1}\inf_{q\in Q_h}\left||p^{n+1}-q_h|\right|^2+\frac{\nu}{12}\left||\nabla\mathcal{D}[\boldsymbol{\phi}_r^{n+1}]|\right|^2. \tag{28}$$

Collecting all of the bounds in (21)-(28) for (20) yields

$$\frac{1}{\Delta t}\left|\left|\begin{bmatrix}\boldsymbol{\phi}_r^{n+1}\\ \boldsymbol{\phi}_r^{n}\end{bmatrix}\right|\right|_G^2-\frac{1}{\Delta t}\left|\left|\begin{bmatrix}\boldsymbol{\phi}_r^{n}\\ \boldsymbol{\phi}_r^{n-1}\end{bmatrix}\right|\right|_G^2+\frac{1}{4\Delta t}\left||\boldsymbol{\phi}_r^{n+1}-2\boldsymbol{\phi}_r^{n}+\boldsymbol{\phi}_r^{n-1}|\right|_F^2$$

$$+\frac{\nu}{2}\left||\nabla\mathcal{D}[\boldsymbol{\phi}_r^{n+1}]|\right|^2+\frac{\nu_T}{2}\left|\left|\widetilde{P}_{\boldsymbol{u},R}\nabla\mathcal{D}[\boldsymbol{\phi}_r^{n+1}]\right|\right|^2$$

$$\leq C\Big((\nu+\nu_T)\left||\nabla\mathcal{D}[\boldsymbol{\eta}^{n+1}]|\right|^2+\nu^{-1}\left||\nabla\mathcal{X}(\boldsymbol{u}_r^n)|\right|^2\left||\nabla\mathcal{D}[\boldsymbol{\eta}^{n+1}]|\right|^2+\nu^{-1}\left||\nabla\mathcal{X}(\boldsymbol{\eta}^n)|\right|^2\left||\nabla\mathcal{D}[\boldsymbol{u}^{n+1}]|\right|^2$$
$$+\nu^{-1}\inf_{q\in Q_h}\left||p^{n+1}-q_h|\right|^2+\nu^{-1}\left|\left|\frac{3\boldsymbol{u}^{n+1}-4\boldsymbol{u}^{n}+\boldsymbol{u}^{n-1}}{2\Delta t}-\boldsymbol{u}_t^{n+1}\right|\right|^2+\nu\left||\nabla(\mathcal{D}[\boldsymbol{u}^{n+1}]-\boldsymbol{u}^{n+1})|\right|^2$$
$$+\nu_T\left|\left|\widetilde{P}_{\boldsymbol{u},R}\nabla\mathcal{D}[\boldsymbol{u}^{n+1}]\right|\right|^2+\nu^{-1}\left||\nabla\mathcal{X}(\boldsymbol{u}^n)|\right|^2\left||\nabla(\mathcal{D}[\boldsymbol{u}^{n+1}]-\boldsymbol{u}^{n+1})|\right|^2$$

$$+\nu^{-1}\left||\nabla(\mathcal{X}(\boldsymbol{u}^n)-\boldsymbol{u}^{n+1})|\right|^2\left||\nabla\boldsymbol{u}^{n+1}|\right|^2\Big)+C\nu^{-1}\left||\nabla\mathcal{X}(\boldsymbol{\phi}_r^n)|\right|\left||\nabla\mathcal{D}[\boldsymbol{u}^{n+1}]|\right|^2. \tag{29}$$

The sum from $n=0\ to\ n=N-1$ and the multiplication of (29) by Δt results in

$$\left|\left|\left|\begin{bmatrix}\boldsymbol{\phi}_r^N\\ \boldsymbol{\phi}_r^{N-1}\end{bmatrix}\right|\right|\right|_G^2+\frac{1}{4}\sum_{n=0}^{N-1}\left||\boldsymbol{\phi}_r^{n+1}-2\boldsymbol{\phi}_r^n+\boldsymbol{\phi}_r^{n-1}|\right|_F^2$$

$$+\frac{\nu\Delta t}{2}\sum_{n=0}^{N-1}\left||\nabla\mathcal{D}[\boldsymbol{\phi}_r^{n+1}]|\right|^2+\frac{\nu_T\Delta t}{2}\sum_{n=0}^{N-1}\left|\left|\widetilde{P}_{\boldsymbol{u},R}\nabla\mathcal{D}[\boldsymbol{\phi}_r^{n+1}]\right|\right|^2$$

$$\leq\left|\left|\left|\begin{bmatrix}\boldsymbol{\phi}_r^0\\ \boldsymbol{\phi}_r^{-1}\end{bmatrix}\right|\right|\right|_G^2+C\Bigg((\nu+\nu_T)\Delta t\sum_{n=0}^{N-1}\left||\nabla\mathcal{D}[\boldsymbol{\eta}^{n+1}]|\right|^2$$

$$+\nu^{-1}\Delta t\sum_{n=0}^{N-1}\left||\nabla\mathcal{X}(\boldsymbol{u}_r^n)|\right|^2\left||\nabla\mathcal{D}[\boldsymbol{\eta}^{n+1}]|\right|^2+\nu^{-1}\Delta t\sum_{n=0}^{N-1}\left||\nabla\mathcal{X}(\boldsymbol{\eta}^n)|\right|^2\left||\nabla\mathcal{D}[\boldsymbol{u}^{n+1}]|\right|^2$$

$$+\nu^{-1}\Delta t\sum_{n=0}^{N-1}\left|\left|\frac{3\boldsymbol{u}^{n+1}-4\boldsymbol{u}^n+\boldsymbol{u}^{n-1}}{2\Delta t}-\boldsymbol{u}_t^{n+1}\right|\right|^2+\nu\Delta t\sum_{n=0}^{N-1}\left||\nabla(\mathcal{D}[\boldsymbol{u}^{n+1}]-\boldsymbol{u}^{n+1})|\right|^2$$

$$+\nu_T\Delta t\sum_{n=0}^{N-1}\left|\left|\widetilde{P}_{\boldsymbol{u},R}\nabla\mathcal{D}[\boldsymbol{u}^{n+1}]\right|\right|^2+\nu^{-1}\Delta t\sum_{n=0}^{N-1}\left||\nabla\mathcal{X}(\boldsymbol{u}^n)|\right|^2\left||\nabla(\mathcal{D}[\boldsymbol{u}^{n+1}]-\boldsymbol{u}^{n+1})|\right|^2$$

$$+\nu^{-1}\Delta t\sum_{n=0}^{N-1}\left||\nabla(\mathcal{X}(\boldsymbol{u}^n)-\boldsymbol{u}^{n+1})|\right|^2\left|\nabla\boldsymbol{u}^{n+1}\right|^2+\nu^{-1}\Delta t\sum_{n=0}^{N-1}\inf_{\mathrm{q}\in\mathrm{Q_h}}\left|p^{n+1}-q_h\right|^2\Bigg)$$

$$+C\nu^{-1}\Delta t\left|\left||\nabla\mathcal{D}[\boldsymbol{u}]|\right|\right|_{\infty,0}^2\sum_{n=0}^{N-1}\left(4\left|\nabla\boldsymbol{\phi}_r^n\right|^2+\left|\nabla\boldsymbol{\phi}_r^{n-1}\right|^2\right). \tag{30}$$

Utilizing the definition of $\boldsymbol{L}_{R,\boldsymbol{u}}$ and $\widetilde{P}_{\boldsymbol{u},R}=I-P_{\boldsymbol{u},R}$, the bound of the seventh term on the right-hand side of (30) can be obtained as:

$$\Delta t\sum_{n=0}^{N-1}\left|\left|\widetilde{P}_{\boldsymbol{u},R}\nabla\mathcal{D}[\boldsymbol{u}^{n+1}]\right|\right|^2=\Delta t\sum_{n=0}^{N-1}\left|\left|\nabla\mathcal{D}[\boldsymbol{u}^{n+1}]-P_{\boldsymbol{u},R}\nabla\mathcal{D}[\boldsymbol{u}^{n+1}]\right|\right|^2$$

$$\leq\frac{\mathrm{C}}{N}\sum_{n=0}^{N-1}\inf_{\boldsymbol{v}_R\in\boldsymbol{X}_R}\left||\nabla\mathcal{D}[\boldsymbol{u}^{n+1}]-\nabla\mathcal{D}[\boldsymbol{v}_R]|\right|^2$$

$$\leq\frac{\mathrm{C}}{N}\sum_{n=0}^{N-1}\left|\left|\nabla\mathcal{D}[\boldsymbol{u}^{n+1}]-\nabla\mathcal{D}[\boldsymbol{U}_R^{n+1}]\right|\right|^2 \tag{31}$$

where $\boldsymbol{U}_R^{n+1}$ denotes the large-scale representation of the projection. By utilizing the approximation properties (3), the Equation (31), Assumption 2.1**,** Lemma 2.2, Lemma 2.6, and Lemma 3.2, the right-hand side terms in (30) can be bounded as

$$\Delta t\sum_{n=0}^{N-1}\left||\nabla\mathcal{D}[\boldsymbol{\eta}^{n+1}]|\right|^2\leq C\left(\left(h^{2s}+\left||\mathcal{S}_r|\right|_2h^{2s+2}\right)\left|\left|\boldsymbol{u}\right|\right|_{2,s+1}^2+\sum_{i=r+1}^{d}\left|\left|\boldsymbol{\psi}_i\right|\right|_1^2\mu_i\right), \tag{32}$$

$$\Delta t\sum_{n=0}^{N-1}\left||\nabla\mathcal{X}(\boldsymbol{u}_r^n)|\right|^2\left||\nabla\mathcal{D}[\boldsymbol{\eta}^{n+1}]|\right|^2$$

$$\leq C\left(\left|\left|\boldsymbol{u}_r^0\right|\right|^2+\left|\left|2\boldsymbol{u}_r^0-\boldsymbol{u}_r^{-1}\right|\right|^2+\left|\left|\boldsymbol{u}_r^0-\boldsymbol{u}_r^{-1}\right|\right|^2+2\nu^{-1}\Delta t\sum_{n=0}^{N-1}\left|\left|\boldsymbol{f}^{n+1}\right|\right|_{-1}^2\right)$$
$$\times\left(\left(h^{2s}+\left|\left|\mathcal{S}_r\right|\right|_2 h^{2s+2}\right)\left|\left|\left|\boldsymbol{u}\right|\right|\right|_{2,s+1}^2+\sum_{i=r+1}^{d}\left|\left|\boldsymbol{\psi}_i\right|\right|_1^2\mu_i\right), \tag{33}$$

$$\Delta t\sum_{n=0}^{N-1}\left|\left|\nabla\mathcal{X}(\boldsymbol{\eta}^n)\right|\right|^2\left|\left|\nabla\mathcal{D}[\boldsymbol{u}^{n+1}]\right|\right|^2$$
$$\leq\ C\left|\left|\left|\nabla\,\mathcal{D}[\boldsymbol{u}]\right|\right|\right|_{\infty,0}^2\left(\left(h^{2s}+\left|\left|\mathcal{S}_r\right|\right|_2 h^{2s+2}\right)\left|\left|\left|\boldsymbol{u}\right|\right|\right|_{2,s+1}^2+\sum_{i=r+1}^{d}\left|\left|\boldsymbol{\psi}_i\right|\right|_1^2\mu_i\right), \tag{34}$$

$$\Delta t\sum_{n=0}^{N-1}\left|\left|\frac{3\boldsymbol{u}^{n+1}-4\boldsymbol{u}^n+\boldsymbol{u}^{n-1}}{2\Delta t}-\boldsymbol{u}_t^{n+1}\right|\right|^2\leq C\Delta t^4\left|\left|\boldsymbol{u}_{ttt}\right|\right|^2_{L^2\left(0,T;L^2(\Omega)\right)}, \tag{35}$$

$$\Delta t\sum_{n=0}^{N-1}\left|\left|\nabla(\mathcal{D}[\boldsymbol{u}^{n+1}]-\boldsymbol{u}^{n+1})\right|\right|^2\leq C\Delta t^4\left|\left|\nabla\boldsymbol{u}_{tt}\right|\right|^2_{L^2\left(0,T;L^2(\Omega)\right)}, \tag{36}$$

$$\Delta t\sum_{n=0}^{N-1}\left|\left|\nabla\mathcal{D}[\boldsymbol{u}^{n+1}]-\nabla\mathcal{D}[\boldsymbol{U}_R^{n+1}]\right|\right|^2\leq\ C\left(\left(h^{2s}+\left|\left|\mathcal{S}_R\right|\right|_2 h^{2s+2}\right)\left|\left|\left|\boldsymbol{u}\right|\right|\right|_{2,s+1}^2+\sum_{i=R+1}^{d}\left|\left|\boldsymbol{\psi}_i\right|\right|_1^2\mu_i\right), \tag{37}$$

$$\Delta t\sum_{n=0}^{N-1}\left|\left|\nabla(\mathcal{X}(\boldsymbol{u}^n)-\boldsymbol{u}^{n+1})\right|\right|^2\leq C\Delta t^4\left|\left|\nabla\boldsymbol{u}_{tt}\right|\right|^2_{L^2\left(0,T;L^2(\Omega)\right)}, \tag{38}$$

$$\Delta t\sum_{n=0}^{N-1}\inf_{\mathrm{q}\in\mathrm{Q_h}}\left|\left|p^{n+1}-q_h\right|\right|\ \leq Ch^{2s}\left|\left|\left|p\right|\right|\right|_{2,s}^2. \tag{39}$$

Substituting (32)-(39) in (30) and using the assumption $\Delta t\leq C\left(\left|\left|\left|\nabla\mathcal{D}[\boldsymbol{u}]\right|\right|\right|_{\infty,0}^2\right)^{-1}$ allows the utilization of Lemma 2.7, which leads to

$$\left|\left|\left|\begin{bmatrix}\boldsymbol{\phi}_r^N\\ \boldsymbol{\phi}_r^{N-1}\end{bmatrix}\right|\right|\right|_G^2+\frac{1}{4}\sum_{n=0}^{N-1}\left|\left|\boldsymbol{\phi}_r^{n+1}-2\boldsymbol{\phi}_r^n+\boldsymbol{\phi}_r^{n-1}\right|\right|_F^2+\frac{\nu\Delta t}{2}\sum_{n=0}^{N-1}\left|\left|\nabla\mathcal{D}[\boldsymbol{\phi}_r^{n+1}]\right|\right|^2+\frac{\nu_T\Delta t}{2}\sum_{n=0}^{N-1}\left|\left|\widetilde{P}_{\boldsymbol{u},R}\nabla\mathcal{D}[\boldsymbol{\phi}_r^{n+1}]\right|\right|^2$$
$$\leq\left|\left|\left|\begin{bmatrix}\boldsymbol{\phi}_r^0\\ \boldsymbol{\phi}_r^{-1}\end{bmatrix}\right|\right|\right|_G^2+C^*\left(1+h^{2s}+\Delta t^4+\left(\left|\left|\mathcal{S}_r\right|\right|_2+\left|\left|\mathcal{S}_R\right|\right|_2\right)h^{2s+2}+\sum_{i=r+1}^{d}\left|\left|\boldsymbol{\psi}_i\right|\right|_1^2\mu_i+\sum_{i=R+1}^{d}\left|\left|\boldsymbol{\psi}_i\right|\right|_1^2\mu_i\right) \tag{40}$$

where C^* depends on ν,ν_T. Applying Lemma 2.4, removing the non-negative terms, and multiplying by 4, one has

$$\left|\left|\boldsymbol{\phi}_r^N\right|\right|^2 + 2\nu\Delta t\sum_{n=0}^{N-1}\left|\left|\nabla\mathcal{D}[\boldsymbol{\phi}_r^{n+1}]\right|\right|^2 + 2\nu_T\Delta t\sum_{n=0}^{N-1}\left|\left|\widetilde{P}_{\boldsymbol{u},R}\nabla\mathcal{D}[\boldsymbol{\phi}_r^{n+1}]\right|\right|^2$$

$$\leq |\boldsymbol{u}^0 - \boldsymbol{u}_r{}^0||^2 + ||2(\boldsymbol{u}^0 - \boldsymbol{u}_r{}^0) - (\boldsymbol{u}^{-1} - \boldsymbol{u}_r{}^{-1})||^2 + ||(\boldsymbol{u}^0 - \boldsymbol{u}_r{}^0) - (\boldsymbol{u}^{-1} - \boldsymbol{u}_r{}^{-1})||^2$$

$$+C^*\left(1 + h^{2s} + \Delta t^4 + \left(\left|\left|\mathcal{S}_r\right|\right|_2 + \left|\left|\mathcal{S}_R\right|\right|_2\right)h^{2s+2} + \sum_{i=r+1}^{d}\left|\left|\boldsymbol{\psi}_i\right|\right|_1^2\mu_i + \sum_{i=R+1}^{d}\left|\left|\boldsymbol{\psi}_i\right|\right|_1^2\mu_i\right). \tag{41}$$

Finally, applying the triangle inequality, we have

$$\left|\left|\boldsymbol{u}^N - \boldsymbol{u}_r^N\right|\right|^2 + 2\Delta t\sum_{n=0}^{N-1}\left(\nu\left|\left|\nabla\mathcal{D}[\boldsymbol{u}^{n+1} - \boldsymbol{u}_r^{n+1}]\right|\right|^2 + \nu_T\left|\left|\widetilde{P}_{\boldsymbol{u},R}\nabla\mathcal{D}[\boldsymbol{u}^{n+1} - \boldsymbol{u}_r^{n+1}]\right|\right|^2\right)$$

$$\leq \left|\left|\boldsymbol{\phi}_r^N\right|\right|^2 + 2\Delta t\sum_{n=0}^{N-1}\left(\nu\left|\left|\nabla\mathcal{D}[\boldsymbol{\phi}_r^{n+1}]\right|\right|^2 + \nu_T\left|\left|\widetilde{P}_{\boldsymbol{u},R}\nabla\mathcal{D}[\boldsymbol{\phi}_r^{n+1}]\right|\right|^2\right)$$

$$+\left|\left|\boldsymbol{\eta}^N\right|\right|^2 + 2\Delta t\sum_{n=0}^{N-1}\left(\nu\left|\left|\nabla\mathcal{D}[\boldsymbol{\eta}^{n+1}]\right|\right|^2 + \nu_T\left|\left|\widetilde{P}_{\boldsymbol{u},R}\nabla\mathcal{D}[\boldsymbol{\eta}^{n+1}]\right|\right|^2\right). \tag{42}$$

Using Lemma 2.2 and substituting (41) in (42) finish the proof.

4. NUMERICAL EXPERIMENTS

This section is reserved for two numerical experiments in which we verify the theoretical findings and expose the effectiveness of the proposed method. The first test presents the convergence rates by scaling the time step Δt, mesh size h, POD cutoff r, VMS cutoff R to confirm Theorem 3.1. In the second test, we compare the energy conservation properties of the proposed time filtered VMS-POD scheme and the unfiltered case. Here, the Algorithm 2.1 is studied in a two-dimensional domain Ω. For all simulations, the flow over a circular cylinder in a 2D channel (please see [4, 18, 20]) is utilized as a test problem which is illustrated in Figure 1.

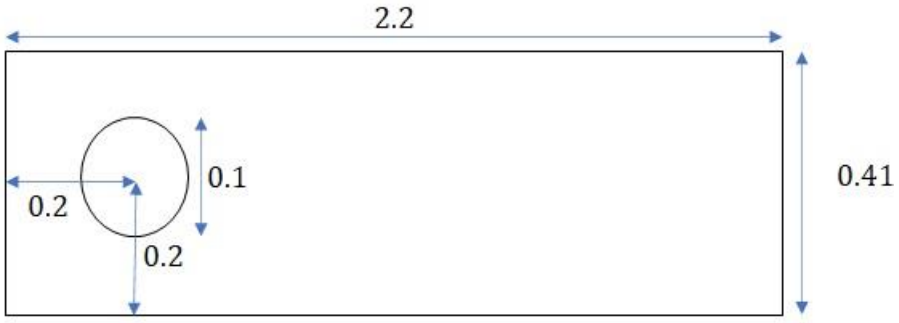

Figure 1. *2D channel flow over a circular cylinder domain*

In the test problem, no-slip boundary conditions are imposed along the walls and cylinder. In addition, the following inflow and outflow boundary conditions are applied:

$$\boldsymbol{u_1}(0,y,t) = \boldsymbol{u}_1(2.2,y,t) = \frac{6y(0.41-y)}{0.41^2}, \qquad \boldsymbol{u}_2(0,y,t) = \boldsymbol{u}_2(2.2,y,t) = 0.$$

The parameters are chosen as $\nu = 10^{-3}$, $\Delta t = 0.02$ and $\boldsymbol{f} = 0$ (no forcing). The POD method collects the snapshots from a BDF2-finite element DNS simulation with Taylor-Hood elements and a 103K mesh resolution at each time step from $t = 6$ to $t = 10$.

4.1. Test 1: Convergence Rates Verification

In this test, our special interest is the scaling of the errors with respect to the time step Δt , mesh size h, POD cutoff r and VMS cutoff R. Here, the true solution is chosen as the BDF2-FEM solution of NSE. First, we scale the numerical error of the proposed method with respect to the time step Δt. We select the parameters as $r = 8,\ R = 5,\ \nu_T = 0{,}0003$, end time $= 4$ to verify the numerical analysis of the Algorithm 2.1. The errors and convergence rates are shown in Table 1 for decreasing values of Δt. To measure the error between the numerical solution and the true solution, we utilize the norm in $L^{\infty}\left(0,\tau;L^{2}(\Omega)\right)$ space which can be expressed as

$$\left|\left|\left|\boldsymbol{u}-\boldsymbol{u}_r\right|\right|\right|_{L^{\infty}\left(L^{2}(\Omega)\right)} := max_{0\le n\le N}\left|\left|\boldsymbol{u}(t^n)-\boldsymbol{u}_r^n\right|\right|_{L^{2}(\Omega)}.$$

Table 1. *Convergence of the filtered VMS-POD for varying* Δt

Δt	$\left\|\left\|\left\|\boldsymbol{u}-\boldsymbol{u}_r\right\|\right\|\right\|_{L^{\infty}(L^{2}(\Omega))}$	rate
0.010	0.45361	-
0.008	0.34680	1.20
0.006	0.25176	1.11
0.004	0.14852	1.30
0.002	0.03804	1.97

We observe that the rates improve to the second order even for the large time step with the use of the filter. The results are consistent with Theorem 3.1. Next, we check the convergence rates for varying mesh size h. To isolate the spatial error, we fix the $\Delta t = 0.02$, end time $= 1, r = 20, R = 12$. The error values, and converegence rates are given in Table 2. It is observed that third order convergence in $L^{\infty}(0,\tau;L^{2}(\Omega))$-norm.

Table 2. *Convergence of the filtered VMS-POD for varying* h

h	$\left\|\left\|\left\|\boldsymbol{u}-\boldsymbol{u}_r\right\|\right\|\right\|_{L^{\infty}(L^{2}(\Omega))}$	rate
0.20	0.4343	-
0.15	0.1564	3.55
0.10	0.0620	2.28
0.05	0.0210	1.56
0.03	0.0031	3.74

As the error estimate depends also on the POD cutoff r and VMS cutoff R via the terms

$$\varepsilon_r = \sum_{i=r+1}^{d}\left|\left|\boldsymbol{\psi}_i\right|\right|_1^2\mu_i\,, \qquad \varepsilon_R = \sum_{i=R+1}^{d}\left|\left|\boldsymbol{\psi}_i\right|\right|_1^2\mu_i,$$

we now verify the convergence rates of the method with respect to different r and R. We choose $\Delta t = 0.002$ and calculate ε_R and ε_r for each r and R. The resultant errors and rates are listed in Tables 3 and 4 for increasing values of R and r, respectively. Here, we use the norm in the $L^{2}\left(0,\tau;H^{1}(\Omega)\right)$ space given by

$$\left|\left|\left|\boldsymbol{u}-\boldsymbol{u}_r\right|\right|\right|_{L^{2}\left(H^{1}(\Omega)\right)} := \sqrt{\Delta t\sum_{n=1}^{N}\left|\left|\boldsymbol{u}(t^n)-\boldsymbol{u}_r^n\right|\right|_{H^{1}(\Omega)}^2}\,.$$

Table 3. *Convergence of the filtered VMS-POD for varying R*

R	R	ε_R	$\left\|\|\|\boldsymbol{u}-\boldsymbol{u}_r\|\|\right\|_{L^\infty(L^2(\Omega))}$	rate	$\left\|\|\|\boldsymbol{u}-\boldsymbol{u}_r\|\|\right\|_{L^2(H^1(\Omega))}$	rate
20	1	52.1231	0.1701	-	5.8665	-
20	3	18.1675	0.0384	1.41	1.5101	1.29
20	5	10.4747	0.0281	0.57	1.2299	0.37
20	7	4.7608	0.0193	0.47	0.8504	0.47

Table 4. *Convergence of the filtered VMS-POD for varying r*

R	R	ε_r	$\left\|\|\|\boldsymbol{u}-\boldsymbol{u}_r\|\|\right\|_{L^\infty(L^2(\Omega))}$	rate	$\left\|\|\|\boldsymbol{u}-\boldsymbol{u}_r\|\|\right\|_{L^2(H^1(\Omega))}$	rate
4	3	13.458	0.2389	-	8.1399	-
6	3	5.4549	0.0898	1.08	4.7426	0.59
8	3	3.4015	0.0442	1.50	2.3595	1.48
10	3	1.5230	0.0283	0.55	1.6768	0.43

We observe that convergence rates with respect to r and R are close to 0.5 in both $L^\infty(0,\tau;L^2(\Omega))$ and $L^2\big(0,\tau;H^1(\Omega)\big)$ norms. The calculated rates are in line with the corresponding values reported in [1, 4].

4.2. Test 2: Conservation of Energy

In the second test, the aim is to show that the global energy

$$Energy = \frac{1}{2}\int_\Omega \boldsymbol{u}(x)\boldsymbol{u}(x)dx$$

is preserved for the solution obtained by the Algorithm 2.1. We also aim to demonstrate that the proposed time filtered VMS-POD method is more successful in predicting the energy compared to the unfiltered case. We choose the parameters as $\Delta t = 0.002, r = 8,\ R = 5, \nu_T = 0{,}0003$, end time $= 4$. At each time step, energy values versus time for both cases are displayed in Figure 2.

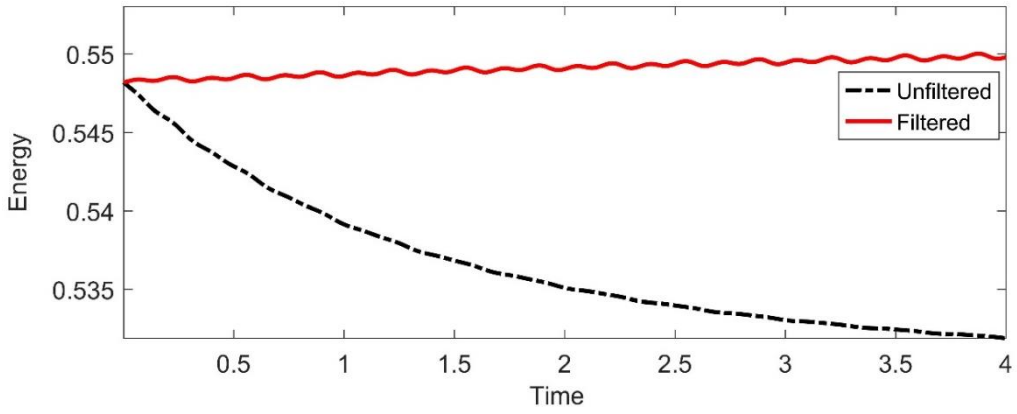

Figure 2. *Energy versus time for unfiltered and filtered case*

In Figure 2, it is seen that the conservation of energy property improves when time filtering is added to the classical backward Euler method. Hence, the proposed time filtered VMS-POD method conserves the energy better than the unfiltered case.

Next, we check the lift and drag coefficients of the filtered VMS-POD approach obtained from 25K, 55K, and 103K degrees of freedom for velocity in FEM simulations. Average and range of the lift and drag coefficients are defined as

$$c_d^{ave}, \qquad c_d^{range} = \left|c_d^{max} - c_d^{min}\right|, \qquad c_l^{ave}, \qquad c_l^{range} = \left|c_l^{max} - c_l^{min}\right|.$$

Here, we take the lift and drag coefficients of DNS simulations as reference and calculate the error between them and c_d^{ave}, c_d^{range}, c_l^{ave} and c_l^{range}. The lift and drag coefficients, as well as the error values for each r are listed in Table 5.

Table 5. *Average and range of lift and drag coefficients for varying r*

r	FEM DOF	c_d^{ave}	error	c_d^{range}	error	c_l^{ave}	error	c_l^{range}	error
	103K	3.18	-	0.07	-	-0.01	-	2.04	-
8	25K	3.18	<0.01	0.09	0.02	-0.01	<0.01	2.12	0.08
8	55K	3.19	0.01	0.08	0.01	-0.01	<0.01	2.07	0.03
8	103K	3.20	0.02	0.10	0.03	-0.01	<0.01	2.13	0.09
10	25K	3.18	<0.01	0.07	<0.01	-0.01	<0.01	2.09	0.05
10	55K	3.19	0.01	0.07	<0.01	-0.01	<0.01	2.05	0.01
10	103K	3.17	0.01	0.08	0.01	-0.01	<0.01	2.04	<0.01
12	25K	3.18	<0.01	0.07	<0.01	-0.01	<0.01	2.10	0.06
12	55K	3.19	0.01	0.07	<0.01	-0.01	<0.01	2.06	0.02
12	103K	3.18	<0.01	0.07	<0.01	-0.01	<0.01	2.05	0.01

Note that, the results in the Table 5 are in line with the results reported in [20].

5. CONCLUSIONS

In this paper, the effectiveness of adding time filters to the VMS-POD method is demonstrated by means of theoretical and computational analyzes. It is shown that the proposed method is energy preserving, unconditionally stable, and convergent. The numerical experiments validate the numerical applicability of the method. In the first test, the convergence rates with respect to $\Delta t, h, r$ and R are examined. The results of this numerical test on the benchmark problem are confirmed with the theoretical findings. In the second test, the effects of the filter to the energy balance properties of the VMS-POD method are evaluated. Results of the second numerical experiment indicate that the addition of the time filter provides better energy saving. In the light of these numerical tests, it has been observed that the filtered VMS-POD method both increases the accuracy and conserves the energy better.

CONFLICTS OF INTEREST

No conflict of interest was declared by the author.

REFERENCES

[1] Eroglu, F., Kaya, S., Rebholz, L., "POD-ROM for the Darcy-Brinkman equations with double-diffusive convection", Journal of Numerical Mathematics, 27(3): 123–139, (2019).

[2] Kunisch, K., Volkwein, S., "Galerkin proper orthogonal decomposition methods for parabolic problems", Numerische Mathematik, 90: 117–148, (2001).

[3] San, O., Borggaard, J., "Principal interval decomposition framework for POD reduced-order modeling of convective Boussinesq flows", International Journal for Numerical Methods in Fluids, 78(1): 37–62, (2015).

[4] Eroglu, F., Kaya, S., Rebholz, L., "A modular regularized variational multiscale proper orthogonal decomposition for incompressible flows", Computer Methods in Applied Mechanics and Engineering, 325: 350–368, (2017).

[5] Eroglu, F., Kaya, S., Rebholz, L., "Decoupled modular regularized VMS-POD for Darcy-Brinkman equations", IAENG International Journal of Applied Mathematics, 49(2): 134–144, (2019).

[6] Iliescu, T., Wang Z., "Variational multiscale proper orthogonal decomposition: Navier-Stokes equations", Numerical Methods for Partial Differential Equations, 30(2): 641–663, (2014).

[7] Iliescu, T., Wang, Z., "Variational multiscale proper orthogonal decomposition: Convection-dominated convection-diffusion-reaction equations", Mathematics of Computation, 82(283): 1357–1378, (2013).

[8] Roop, J. P., "A proper-orthogonal decomposition variational multiscale approximation method for a generalized Oseen problem", Advances in Numerical Analysis, 2013: 1–8, (2013).

[9] Cibik, A., Demir, M., Kaya, S., "A family of second order time stepping methods for the Darcy-Brinkman equations", Journal of Mathematical Analysis and Applications, 472(1): 148–175, (2019).

[10] Guzel, A., Layton, W., "Time filters increase accuracy of the fully implicit method", BIT Numerical Mathematics, 58: 301–315, (2018).

[11] Akbas, M., "An adaptive time filter based finite element method for the velocity-vorticity-temperature model of the incompressible non-isothermal fluid flows", Gazi University Journal of Science, 33(3): 696–713, (2020).

[12] Cibik, A., Eroglu, F., Kaya, S., "Analysis of second order time filtered backward Euler method for MHD equations", Journal of Scientific Computing, 82: 38, (2020).

[13] DeCaria, V., Layton, W., Zhao, H., "A time-accurate, adaptive discretization for fluid flow problems", International Journal of Numerical Analysis and Modeling, 17(2): 254–280, (2020).

[14] Adams, R., "Sobolev spaces", Academic Press, Newyork, (1975).

[15] Layton, W., "Introduction to the numerical analysis of incompressible viscous flows", Society for Industrial and Applied Mathematics (SIAM), Philadelphia, USA, (2008).

[16] Jiang, N., Mohebujjaman, M., Rebholz, L., Trenchea, C., "An optimally accurate discrete regularization for second order timestepping methods for Navier-Stokes equations", Computer Methods in Applied Mechanics and Engineering, 310: 388–405, (2016).

[17] Trenchea, C., "Second-order unconditionally stable IMEX schemes: Implicit for local effects and explicit for nonlocal effects", ROMAI Journal, 12: 163–178, (2016).

[18] Schäfer, M., Turek, S., "Benchmark computations of laminar flow around a cylinder", In: Hirschel E.H. (eds) Flow Simulation with High-Performance Computers II. Notes on Numerical Fluid Mechanics (NNFM), Vieweg+Teubner Verlag, 48: 547–566, (1996).

[19] Heywood, J., Rannacher, R., "Finite element approximation of the nonstationary Navier-Stokes problem, Part II: Stability of solutions and error estimates uniform in time", SIAM Journal on Numerical Analysis, 23: 750–777, (1986).

[20] Mohebujjaman, M., Rebholz, L., Xie, X., Iliescu, T., "Energy balance and mass conservation in reduced order models of fluid flows", Journal of Computational Physics, 346: 262–277, (2017).